COO-2576-6

ELASTIC AND PLASTIC STRAINS AND THE STRESS CORROSION CRACKING OF AUSTENITIC STAINLESS STEELS

Progress Report
for Period April 30, 1977 - December 30, 1977

A. R. Troiano

Case Western Reserve University
Cleveland, Ohio 44106

January 1978

Prepared For

THE U. S. ENERGY RESEARCH AND DEVELOPMENT ADMINISTRATION
UNDER CONTRACT NO. E- (11-1) - 2576

DISCLAIMER

ABSTRACT

A newly developed test environment based on NaCl, Na_2SO_4 and HCl has provided some insight to several aspects of SCC in a transformable austenitic stainless steel. Current vs. time curves indicated the presence of the formation of a "protective" film which drastically reduced the anodic current leading to failure. This film, not indicated by the polarization curves, is subject to highly localized damage such as pitting. Thus, although it allows only very small corrosion currents, it is not truly protective. Hence, it is pseudo-passive.

The critical cracking potential did not exhibit any difference between the annealed and the maximum (25%) deformation examined. The corrosion or open circuit potential for both annealed and deformed material behaved in a similar manner, becoming more noble with time until it reached the critical cracking potential and SCC ensured. The failure time for the deformed specimens was substantially shorter than for the annealed ones, but the incubation time was essentially the same.

Within the range of experimental conditions examined thus far, it appears that the critical parameters leading to SCC in a chloride environment are primarily dependent on surface-environment interactions and not dependent on the bulk properties.

INTRODUCTION

As indicated in the proposal for continuation of this study (1), a significant portion of the recent research program has been concerned with the "design" of an appropriate test environment for the study of the influence of deformation on stress corrosion cracking of austenitic stainless steels. In the last report it was suggested that the more extensively used boiling $MgCl_2$ solution may possibly be masking some of the more subtle influences of deformation on the electrochemical parameters (2). This conclusion was based on the observation that the critical electrochemical parameters (E_{oc}- open circuit potential, E_{cc}- critical cracking potential, E_{+-} the potential where the current changes from anodic to cathodic) were identical for one particular composition, regardless of the amount of deformation or induced deformation martensite. In particular, the current was always anodic and the open circuit potential always more noble than the critical cracking potential leading to failure. It has been further proposed that this insensitivity of the electrochemical parameters to the structure of the bulk suggested that the phenomenon of localized attack such as pitting is under surface condition control.

This progress report will be divided into two parts. The first part will deal with an extensive analysis of various NaCl, Na_2SO_4, and HCl solutions in an attempt to relate chloride ion concentration, passivating sulphate ions and pH to SCC. The second section deals with the

implementation of the finally selected "optimum" test solution in the study of the influence of deformation on the SCC characteristics of a transformable austenitic stainless steel, type 301.

EXPERIMENTAL

The chemical analysis of the 301 austenitic stainless steel used throughout this investigation is given in Table 1. The alloy in the annealed condition was utilized in the exploratory determination and design of an optimum stress corrosion cracking environment.

The influence of deformation on the .2% offset yield strength and the amount of martensite formed by room temperature deformation is presented in Table 2 and in Figures 1 and 2. Specimens having various amounts of deformation, were loaded to 70% of their respective yield strengths. The testing techniques for SCC experiments have been described previously and do not need to be repeated here (2). Loads as well as potentials were applied within one hour of immersion after the solution had come to a boil and attained an intermediate rest potential which persists for several hours.

Preliminary studies showed that boiling effectively deaerated the solutions, even without deaeration by nitrogen purging. All tests were conducted in the deaerated condition, accomplished by continuous purging of nitrogen as well as boiling.

Polarization curves were determined using a sweep rate of 500 mV per hour. These curves were generated after approximately one hour of immersion for consistency in relating failure curves with the polarization data. All of the potentials listed throughout this study are with reference to the standard calomel electrode (SCE).

RESULTS AND DISCUSSION

Section A: The Test Environment

At this time it may be useful to list and identify again, the various electrochemical parameters and other significant relationships discussed in this report. They are:

E_{oc} - Open Circuit Potential or Corrosion Potential

E_{cc} - Critical Cracking Potential

E_b - Breakdown Potential

E_{+-} - Potential where current shifts from anodic to cathodic.

E_{RP} - Repassivation Potential

E_{oc} vs. Time

I, (Current) vs. Time

Failure Time; open circuit

Failure Time; applied potential

A systematically chosen series of test solutions containing various amounts of NaCl, Na_2SO_4 and HCl were examined. The formulation of this solution from these three constituents has the advantage of examining the effects of the damaging chloride ion, the passivating effect of the sulphate ion and the reduction of pH, individually and without the introduction of extraneous ions.

Some 70 different solutions were examined and polarization curves were run for all solutions. Other tests were conducted on selected solutions of potential interest, as indicated by the polarization curves. Of these curves, a dozen or so are included in this report to indicate significant trends.

The initial studies involved relatively low concentration NaCl solutions. Although all solutions examined displayed active-passive behavior, SCC tests did not result in SCC or pitting attack under open circuit or applied potential conditions active to the breakdown potential (E_b) at these low chloride concentrations. One curve, characteristic of a number of such type curves, shown in Figure 3, displays many of the characteristics present at low NaCl concentrations. The passive region exists over a wide range of potential, extending 400 mVs from the region of electrochemical instability to the E_b. One feature of interest present in this figure which is occasionally observed and reported in the literature is the existence of a cathodic loop at the primary passivation potential (E_p). This is merely a manifestation of the relative magnitudes of the reduction and oxidation partial currents in the potential region of instability.

The inability of these low chloride environments to induce SCC led to an examination of progressively increasing NaCl solutions at a constant value of Na_2SO_4 at .05M (.65%) and pH maintained at 1.0 to 1.5. The boiling temperature of these solutions varied from 100 to 105°C. It is apparent in Figures 4-9 that increasing the chloride concentration reduced passivity, indicated by the shift of E_b in the active direction. This is in agreement with the

generally accepted role assigned to the adsorbed chloride ion.

The influence of the sulfate ion was examined at high chloride concentrations. Figure 10 presents a polarization curve for an unmodified 24% NaCl boiling (107°C) solution, which displays essentially active behavior with only a slight indication of passivity. Figure 11 clearly indicates that the addition of .15 Molar (1.8%) Na_2SO_4 results in the existence of a passive region. This indicates that even at high chloride content, the sulfate ion is competitively adsorbing with the chloride ion and reducing attack.

The reduction in pH in the high chloride solutions proved to provide the most significant modification in terms of the design of the desired test environment. A comparison of figures 10 to 14 indicate the nature of the changes in the polarization curves with large reductions in pH. For example, the curve in Figure 11 obtained in a solution of pH 6.05 compared with the curve in Figure 14, for the same solution but pH .35 is most dramatic. The reduction of pH quite evidently reduces apparent passivity, even in the presence of the protective sulphate ion.

The curve of Figure 13 determined in a low pH solution, indicates the development of a protective film in the potential range of -350 to -400 mV. On the other hand, there is no such indication in the curve of Figure 14 taken in a very low pH environment. However, in a number of cases, SCC test specimens held at potentials where the polarization curves exhibited essentially active behavior, the presence

of some type of protective film was visually obvious.

This raises the question of the ability of polarization curves alone to determine the extent of film formation. Indeed, these potential vs. current curves are determined at specified and usually moderately fast sweep rates and rarely indicate equilibrium conditions. Also, they represent net changes and thus do not give an indication of the intensity of localized attack, if any, as compared to mild general attack. However, current vs. time curves unequivocally and quantitatively indicate the formation of a film with time. Compare, for example, Figures 14 and 15, for the annealed 301 steel in the same environment. Although the polarization curve of Figure 14 gives no indication of film formation, the current-time curve of Figure 15 shows that the current becomes anodic and decreases to very low values as the film forms and in this case at -370 mV applied potential eventually results in failure. The fact that the film takes time to develop explains why the polarization curve does not normally indicate its formation. The anomaly relating the formation of a "protective" film with failure is quite explicable on the basis of the need for a film, highly susceptible to localized attack; that is a pseudo-passive film. Such a film can be defined as one providing general protection as evidenced by the low current (see Figure 15) but subject to highly localized attack usually but not necessarily visually evident in the form of pits. It is significant to point out that a true passive, completely protective film such as shown in Figures 3 or 4, for example, is entirely different in character than the pseudo-passive film discussed above.

Indeed, during the course of assessing the value of various solutions, a number of SCC tests were conducted at potentials in the range indicating passivity. For example, referring to Figure 3, a SCC test at a controlled potential of -250 mV had not failed when the test was ended at 240 hours. Of course, this is not surprising in view of the well-established principle of anodic protection, but it does clearly point out the difference between a true passive and a pseudo-passive film.

The environment finally selected for the further studies, comprised an aqueous solution containing 4.9 M NaCl, .15 M Na_2SO_4, and 3.0 ml HCl per liter, with pH approximately .6. This selection was made largely on the basis of the relatively short times involved in determining the SCC characteristics, we well as the manner in which it pinpoints the pseudo-passive film and its general flexibility.

Section B: Deformation Studies

The critical electrochemical parameters, and basic metallurgical parameters of annealed and cold rolled 301 austenitic stainless steel were determined in the new environment. Failure time vs. potential curves were obtained in order to determine E_{cc} in both the annealed and the 25% cold rolled condition. Table 3 gives the applied potentials, pH initial and final, time to fail, and failure characteristics. Figures 16 and 17 summarize the potential-failure data and indicate a critical cracking potential (E_{cc}) of -370 mV for the annealed condition and -380 mV for the 25% deformed specimens containing approximately 22% deformation martensite (Figure 2). These two potentials are well within the range of experimental error and thus it must be definitely concluded that there is no difference in E_{cc} despite the sub-

stantial difference in the bulk characteristics of the annealed and deformed conditions. This is true, at least for deformations up to 25%.

As indicated earlier (see Figure 15) the currents were initially high and decayed to low anodic values as the pseudo-passive film developed leading to failure. On the other hand at potentials close to E_{cc}, if the current shifted to cathodic values failure did not occur as shown in Figure 18. This behavior of current indicates that E_{cc} and E_{+-} are the same. Figures 15 and 18 give results for the annealed condition and Figures 19 and 20 show essentially the same behavior for the 25% deformed state.

There is a change in the mode of failure depending upon how noble the applied potential is relative to E_{cc}. Specifically, for applied potentials at or only slightly more noble than E_{cc}, the failure mode is clearly cracking. However, as this potential is applied at increasingly more noble values, the cracking becomes less evident and eventually failure appears to occur by simple pitting disintegration.

This change in failure characteristics suggests that there exists a kinetic competition between pitting disintegration and cracking with pitting. Severe pitting attack is favored under conditions producing higher anodic currents and shorter failure times and cracking is favored under longer failure time conditions. Thus, the failure-time curves do not necessarily represent conditions of true SCC over their total range although they are smooth curves. This phenomenon has been reported for a different chloride environment (3). The precise reason for this behavior is not

apparent, however, aside from the greater severity engendered by the more noble potentials, the time sequence for the formation of the pseudo-passive film may also be involved.

As indicated earlier in this report, failure tests employing applied potentials indicated E_{cc} to be -370 to -380 mV. Of course, practical conditions of SCC do not involve potentiostatic control of the potential; rather the component sees the environment and the potential seeks its own E_{oc} (corrosion potential) level. If the approximate value of E_{cc} is near -375 mV, then SCC should occur when the potential shift attains this value. Indeed, it has been demonstrated that failure occurs when E_{oc} becomes equal to or nore noble than E_{cc}(4).

The potential time curves of Figures 21-23 clearly indicate that the potential shifts in the more noble direction after a relatively long period of time at near -450 mV. It is also apparent that SCC occurred when the potential attained the value of -375 mV, consistent with the applied potential determinations of E_{cc} equal -375 mV.

Table 4 summarizes the open circuit test results for both the annealed and cold worked conditions indicating the same basic type of behavior for both of these conditions. In addition, it appears that although there is a substantial difference in total failure time (see Figure 24) the incubation times are essentially the same for the annealed and cold worked conditions. Again, we have an indication that the electrochemical phenomena initiating SCC are independent of the bulk characteristics of the steel which vary widely from the annealed to the deformed material. One must conclude that the initiation of SCC is entirely the result of surface-environment interactions. This is somewhat surpris-

ing considering other results reported in the literature indicating that deformation of transformable austenitic stainless steels very definitely influenced the SCC characteristics (5) (6). However, it is quite possible that the 25% maximum deformation employed thus far in this study may not have been enough for any variation to occur or possibly that loading to 70% of the yield strength was not sufficient to indicate these effects of deformation and/or ferrite (martensite).

An important feature, uniquely present in this environment, is the delayed and then rapid (several minutes) shift of E_{oc} in the more noble direction apparently setting the stage for the approach to E_{cc} and SCC failure. Figures 21 and 22 give E_{oc} as a function of time under stress for both the annealed and deformed specimens. Obviously, the basic characteristics are much the same for both conditions, although deformation substantially accelerates the time to fail, see Figure 24.

Visual observation during these open circuit tests indicated copious hydrogen gas evolution from the entire surface indicating active behavior. The shift to more noble potentials is accompanied by cessation of hydrogen evolution, indicating the formation of a film; in this case, the pseudo-passive film---the precursor to SCC. The discontinuities that occur throughout the propagation, particularly evident in the deformed specimens (Figure 21) is explicable on the basis of the alternate exposure and repassivation of metal surface during the propagation of the crack. Since these are constant load tests, each extension of a crack raises the applied stress accordingly.

In order to determine the extent to which the characteristics of the E_{oc}-time curves may be the result of the stress, the E_{oc} vs. time was monitored with no applied stress. It is clear from the curve of Figure 23, that the E_{oc} vs. time characteristics are independent of the stress. Surprisingly, even the sharp, almost discontinuous shift in the noble direction does not require stress. In as far as the author knows, this phenomenon is completely unique, and may be related to a transformation in the surface film building up to the pseudo-passive state.

Summary Conclusions

1. A test environment has been developed which allows an examination of significant parameters involving SCC in relatively short times. An important aspect of the new test solution involves variations of pH with critical values of less than one.

2. Although polarization curves clearly identified ranges of true passivity, they did not exhibit any indication of the pseudo-passive film.

3. The development of the pseudo-passive film, the precursor to SCC, was clearly indicated by current-time curves, where the current shifted to very low anodic values prior to failure. Visual observation usually confirmed the presence of some type of film.

4. There was no difference in the critical cracking potential for the annealed and the 25 percent cold rolled specimens.

5. The open circuit potential shifted to more noble values with time. When it attained the value equal to the critical cracking potential SCC occurred. There was no essential difference in this behavior for either the annealed or 25 percent deformed state.

6. Although the failure times for the deformed specimens were substantially shorter than for the annealed ones, the incubation times appeared to be essentially the same.

References

1. A. R. Troiano, Proposal, DOE, COO-2576-5, May, 1977.

2. A. R. Troiano, Progress Report, DOE, COO-2576-4 May, 1977

3. K. Kowaka and T. Kudo, U.S.A. - Japan Seminar Proceeding, NACE p. 183, 1976

4. H. H. Uhlig and E. W. Cook, Jr., Jour. Electrochem. Soc., Electrochemical Science, Feb. 1969.

5. I. Matsushima, D. Deegan and H. H. Uhlig, Corrosion, Vol. 22, p. 23, 1966.

6. H. H. Uhlig and R. A. White, Trans. ASM Vol. 52, pg. 830, 1960.

Table 1

Chemical Composition (%)

Cr	Ni	Mo	C	Mn	P	S	Si	Fe
17.95	7.20	0.18	0.094	1.02	.014	.017	0.70	bal

Table 2

.2% Offset Yield Strength and % Martensite

% Def	Y.S. (KSI)	% Martensite
0	46.0	0
11	106.0	3
15	120.7	12
18.5	138.8	17
25	166.2	> 20

Table 3

Applied Potential Data, Annealed and 25% Cold Rolled, 4.9 M NaCl, .15 M Na_2SO_4, 3 ml HCl/1t, 107°C, De.

% Def.	Appl. Pot. (mV SCE)	Initial pH	Final pH	Initial Eoc (mV SCE)	Time to Fail (hrs)	Comments
0	-350	.6	---	-450	6.3	heavily pitted, current positive
0	-360	.5	1.65	-450	23.0	cracked?, current positive
0	-380	.6	1.20	-443	NF(170)	current positive → negative
0	-400	.75	1.15	-440	NF(120)	current positive → negative
25	-370	.7	1.45	-450	2.2	cracked?, current positive
25	-380	.7	---	-454	6.4	cracked, current positive
25	-380	.6	0.90	-450	55.3	cracked, current positive
25	-390	.6	0.90	-450	NF(110)	current positive → negative

Table 4

SCC Tests, Open Circuit, Annealed and Cold Rolled,

4.9 M NaCl, .15 M Na_2SO_4, 3 ml HCl/1t, 107°C, De.

% Def	Initial Eoc (MV SCE)	Final Eoc (MV SCE)	Initial pH	Final pH	Time to Fail (hrs)	Time for Eoc shift hrs.	Comments
0	-442	-380	.35	1.60	35.3	---	SCC secondary cracks
0	-450	-380	.75	1.45	33.5	11.0	SCC secondary cracks
0	-443	-375	.70	1.45	24.9	8.0	SCC secondary cracks
0	-440	-375	.70	1.20	23.5	8.5	SCC secondary cracks
15	-450	-372	.65	1.25	16.5	7.3	SCC single crack
25	-455	-370	.75	1.45	9.7	---	SCC single crack
25	-443	-370	.85	1.35	12.0	8.0	SCC single crack
25	-450	-375	.50	1.30	9.0	6.0	SCC single crack

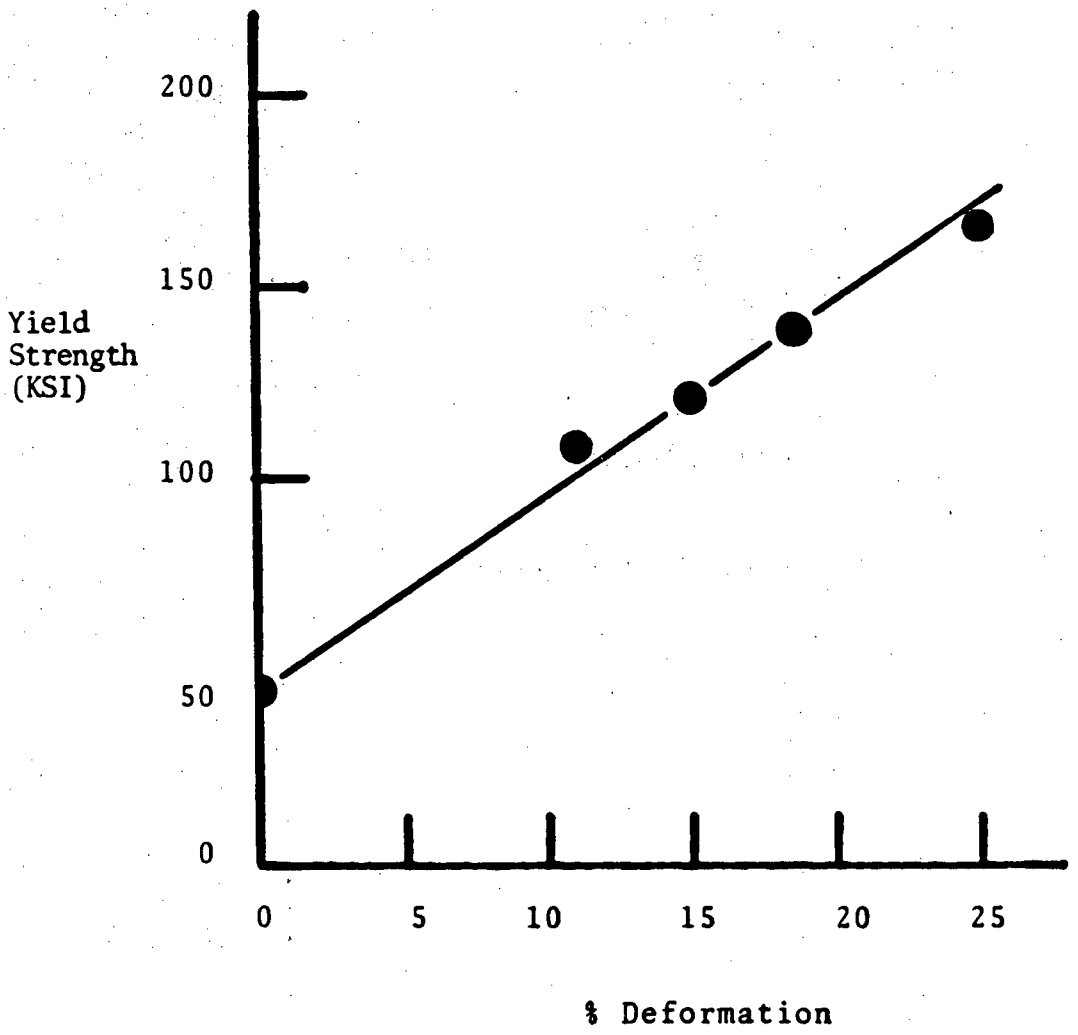

Fig. 1: Yield Strength vs. % Deformation.

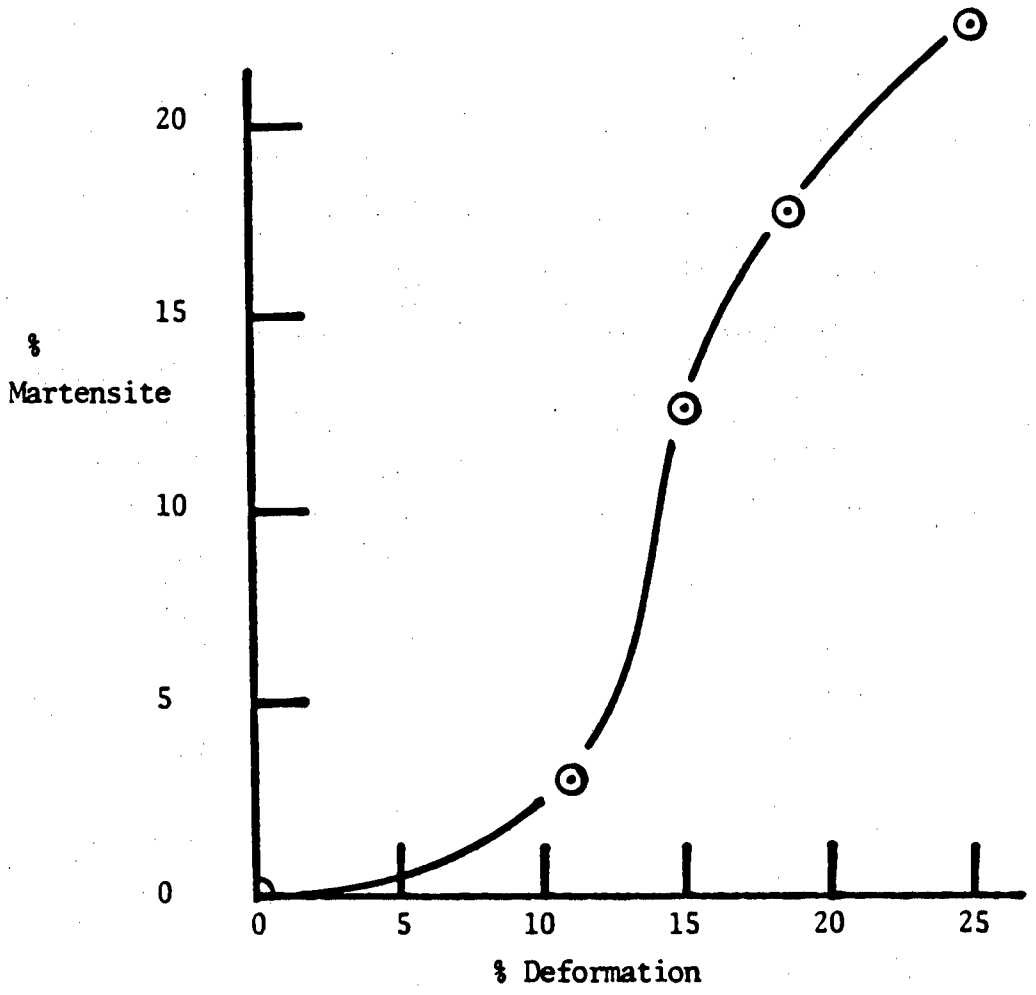

Fig. 2: % Martensite vs. % Deformation.

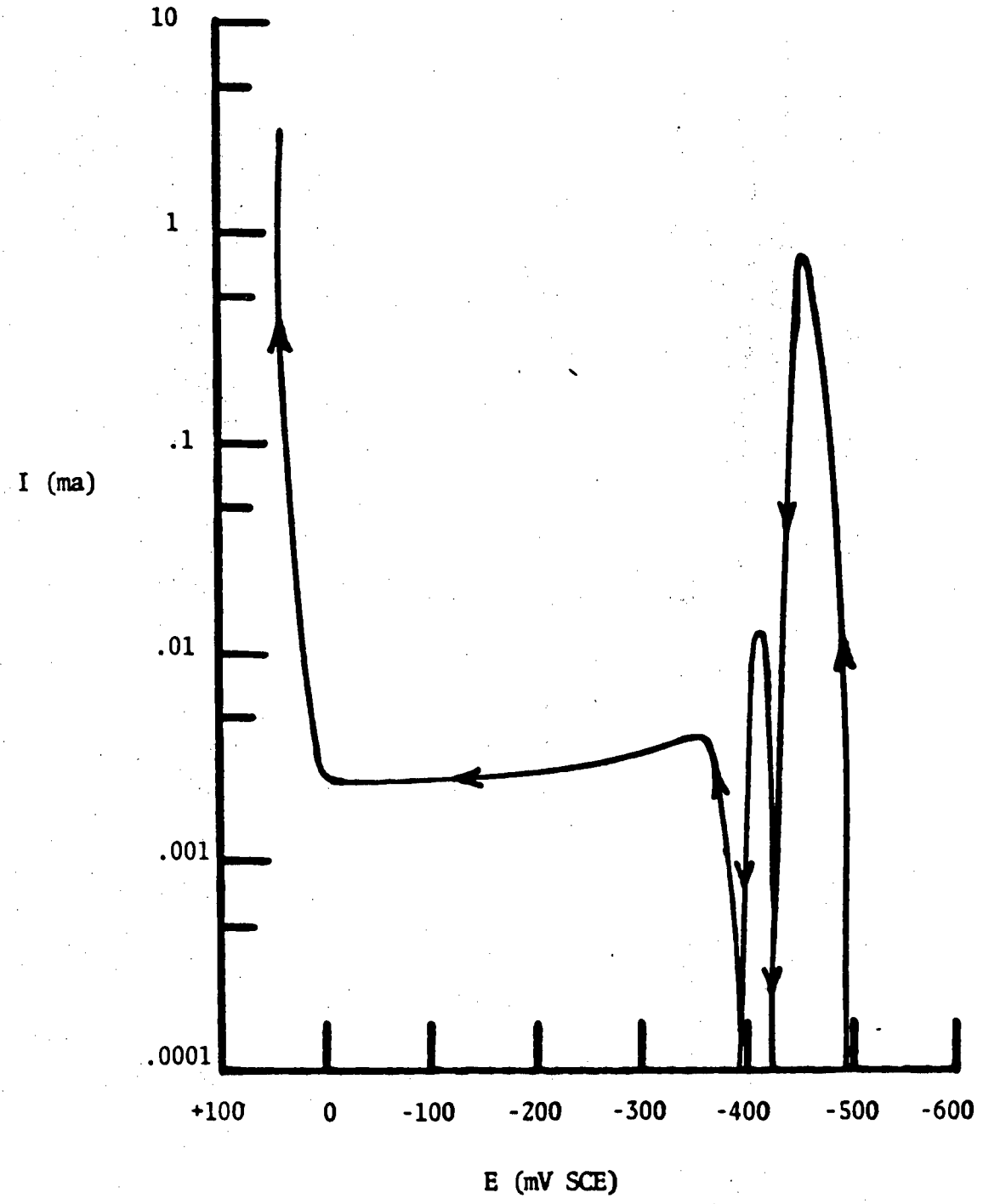

Fig. 3: Polarization Curve. .1M NaCl, .15M Na_2SO_4, .5 ml HCl/1t, pH = 2.1, 100°C.

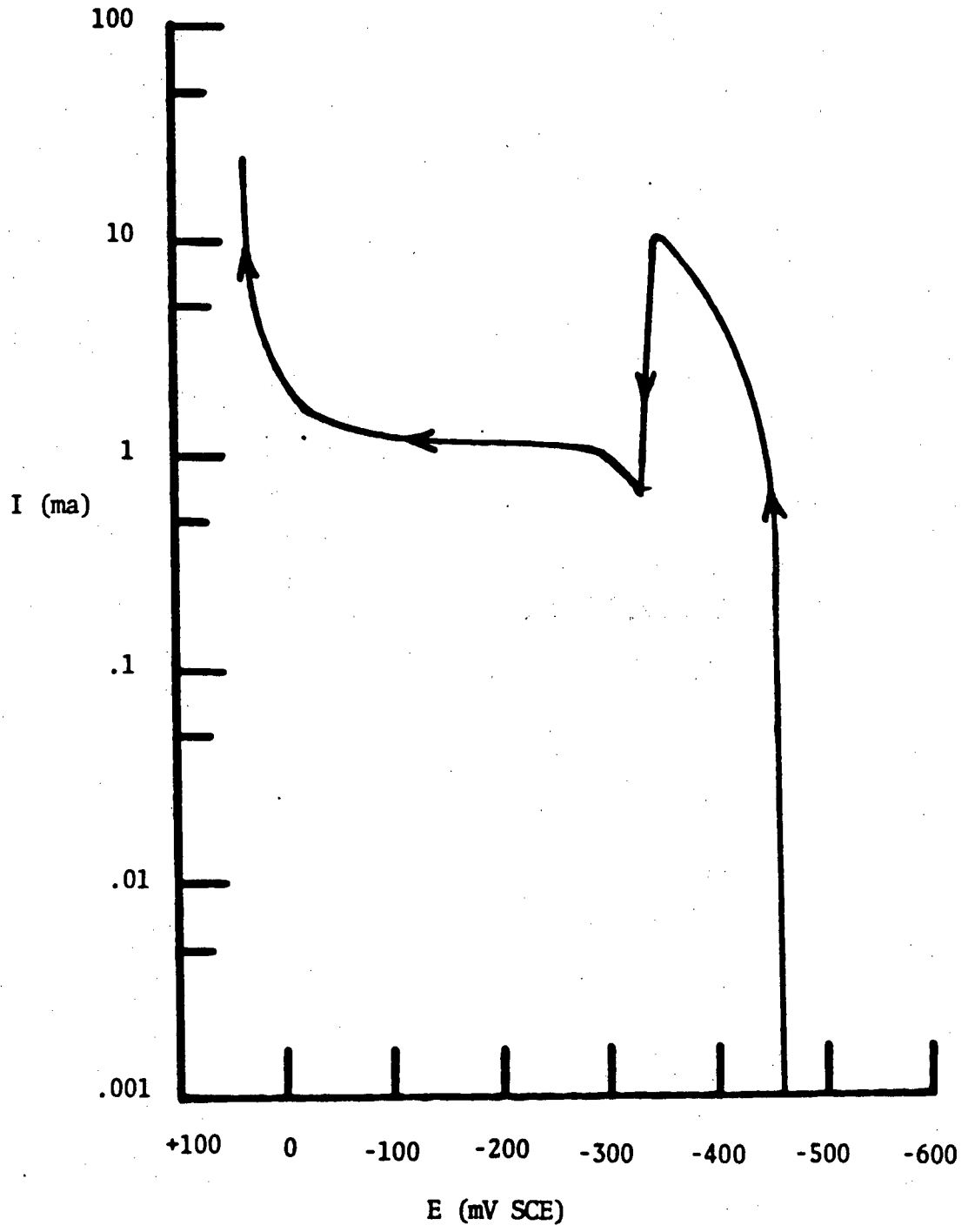

Fig. 4: Polarization Curve; .5M NaCl, .05M Na_2SO_4, pH = 1.5, 100°C.

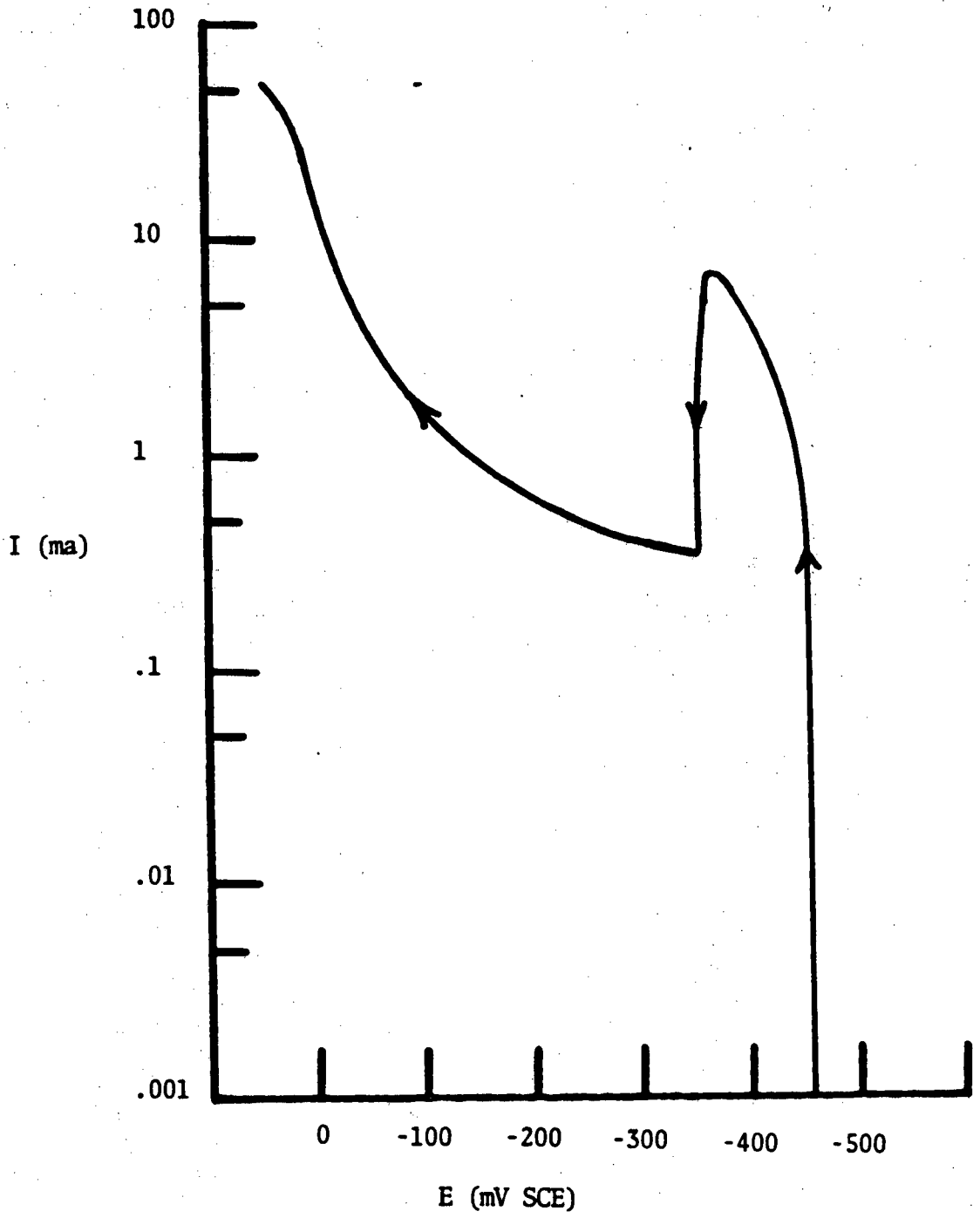

Fig. 5: Polarization Curve; 1.0M NaCl, .05M Na_2SO_4, pH 1.5, 100°C.

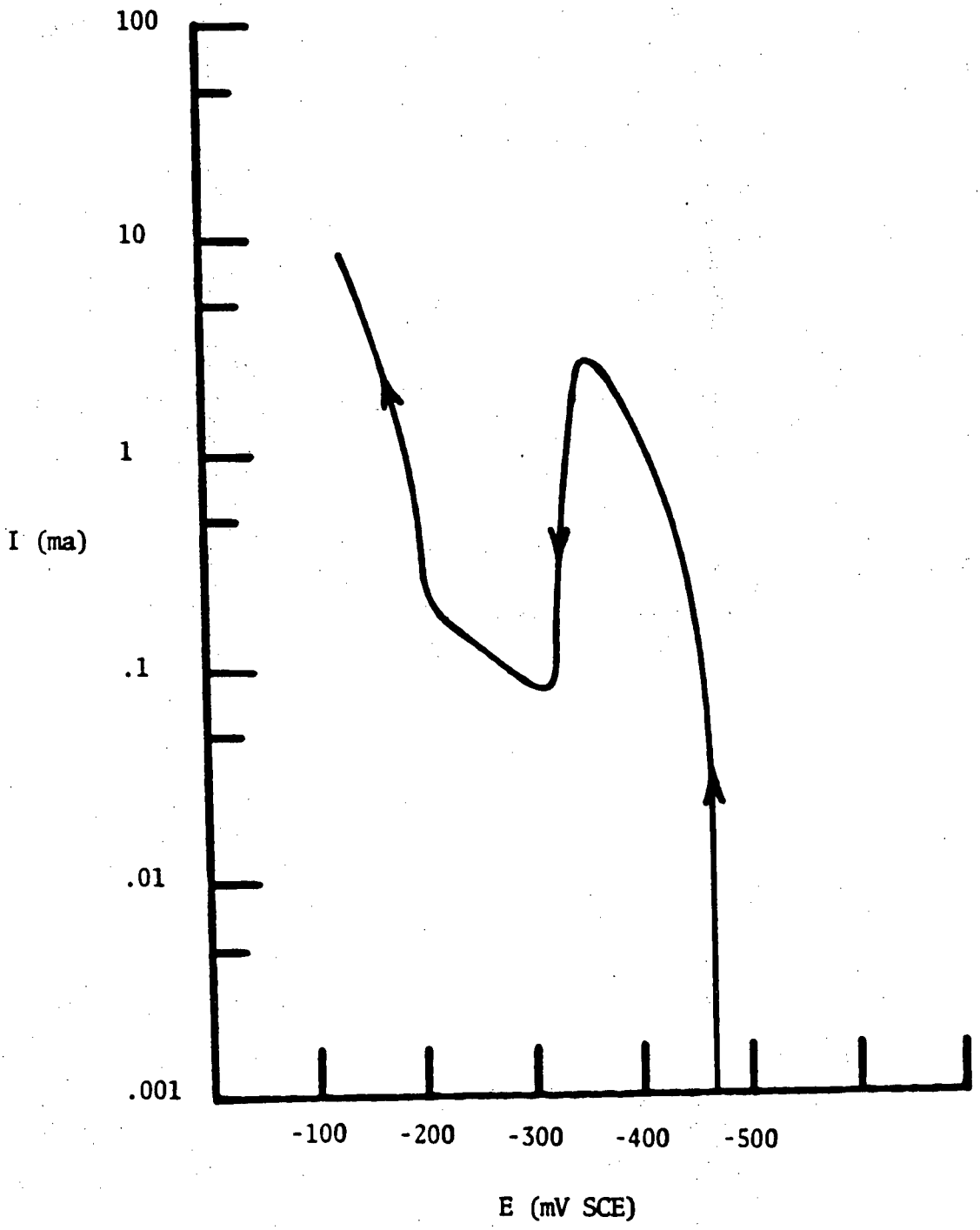

Fig. 6: Polarization Curve; 1.8M NaCl, .05M Na_2SO_4, 3.0 ml HCl/1t, pH = 1.05, 103°C.

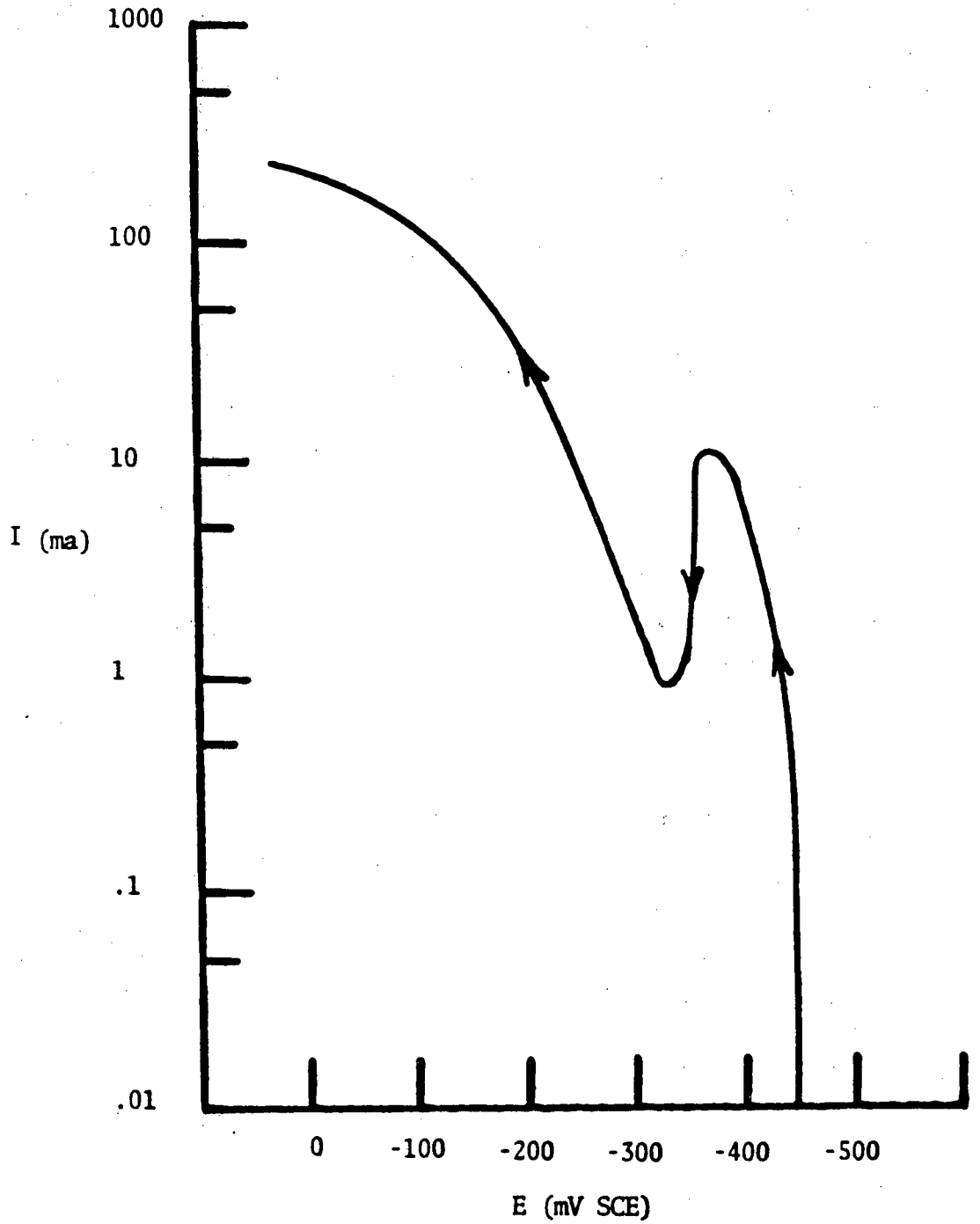

Fig. 7: Polarization Curve; 2.0M NaCl, .05M Na_2SO_4, 2.0 ml HCl/1t, pH = 1.45, 103°C.

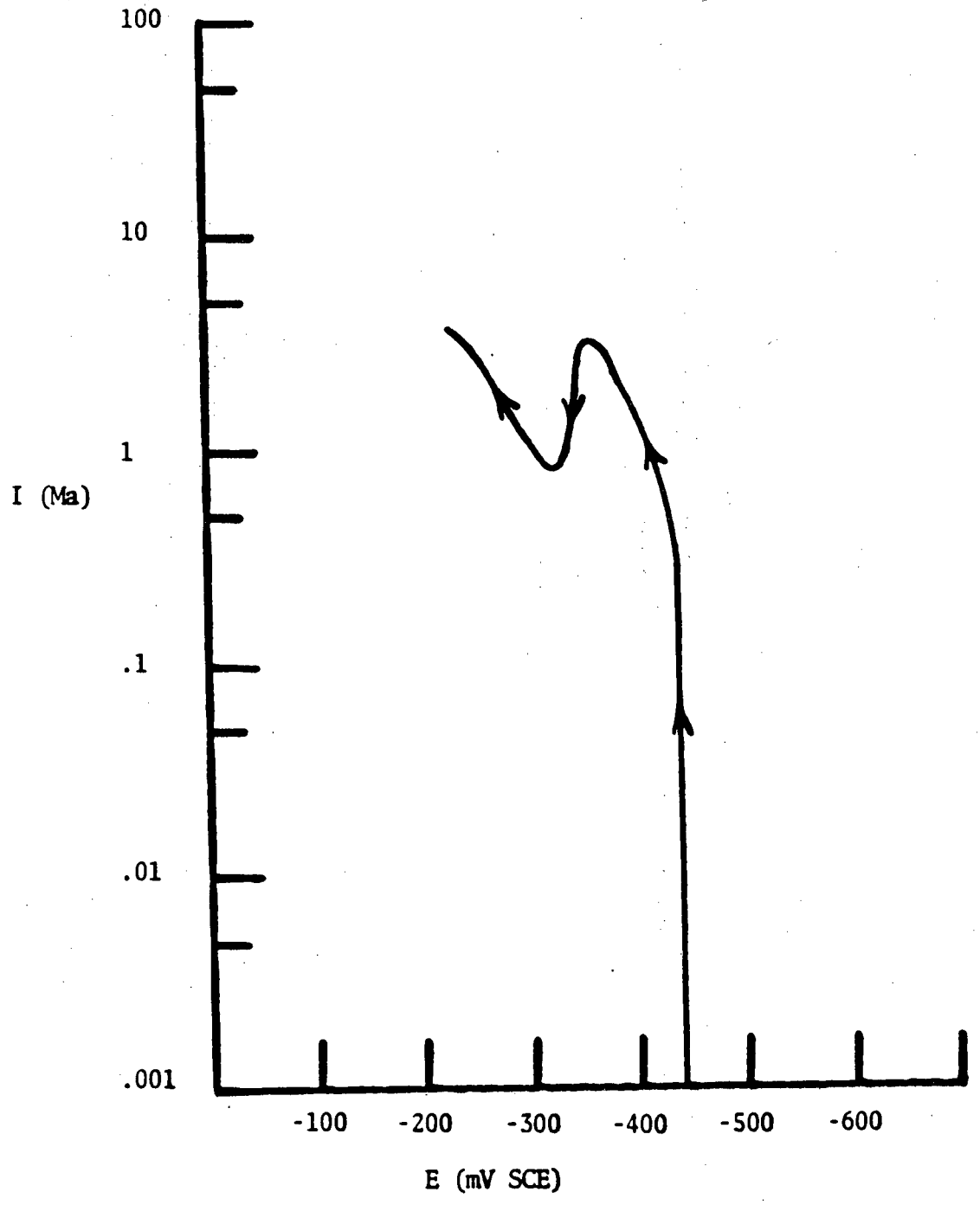

Fig. 8: Polarization Curve; 2.9M NaCl, .05M Na_2SO_4, 3.0 ml HCl/1t, pH = 1.15, 103°C

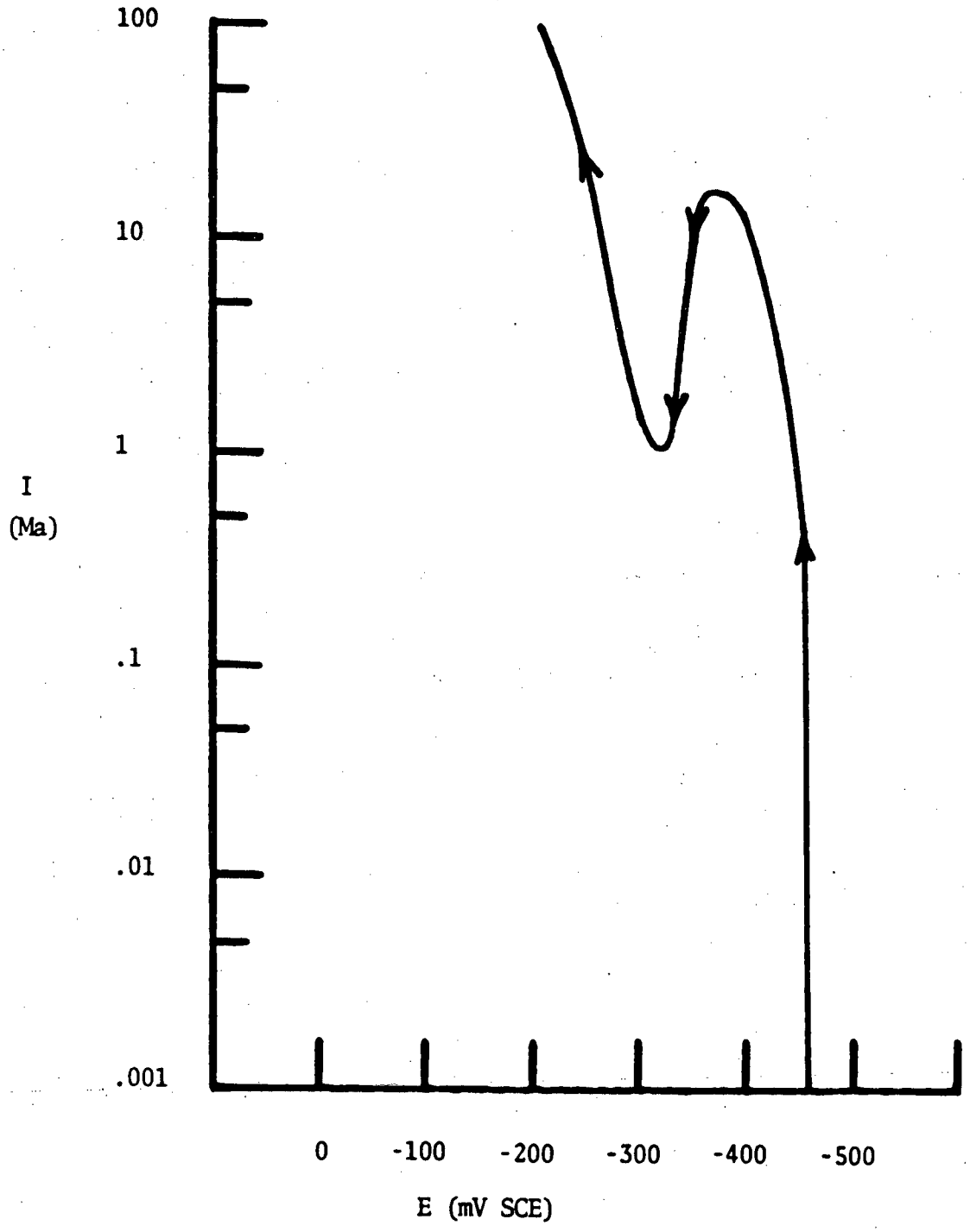

Fig. 9: Polarization Curve; 3.9M NaCl, .05M Na_2SO_4, 1.0 ml HCl/15, pH = 1.25, 105°C.

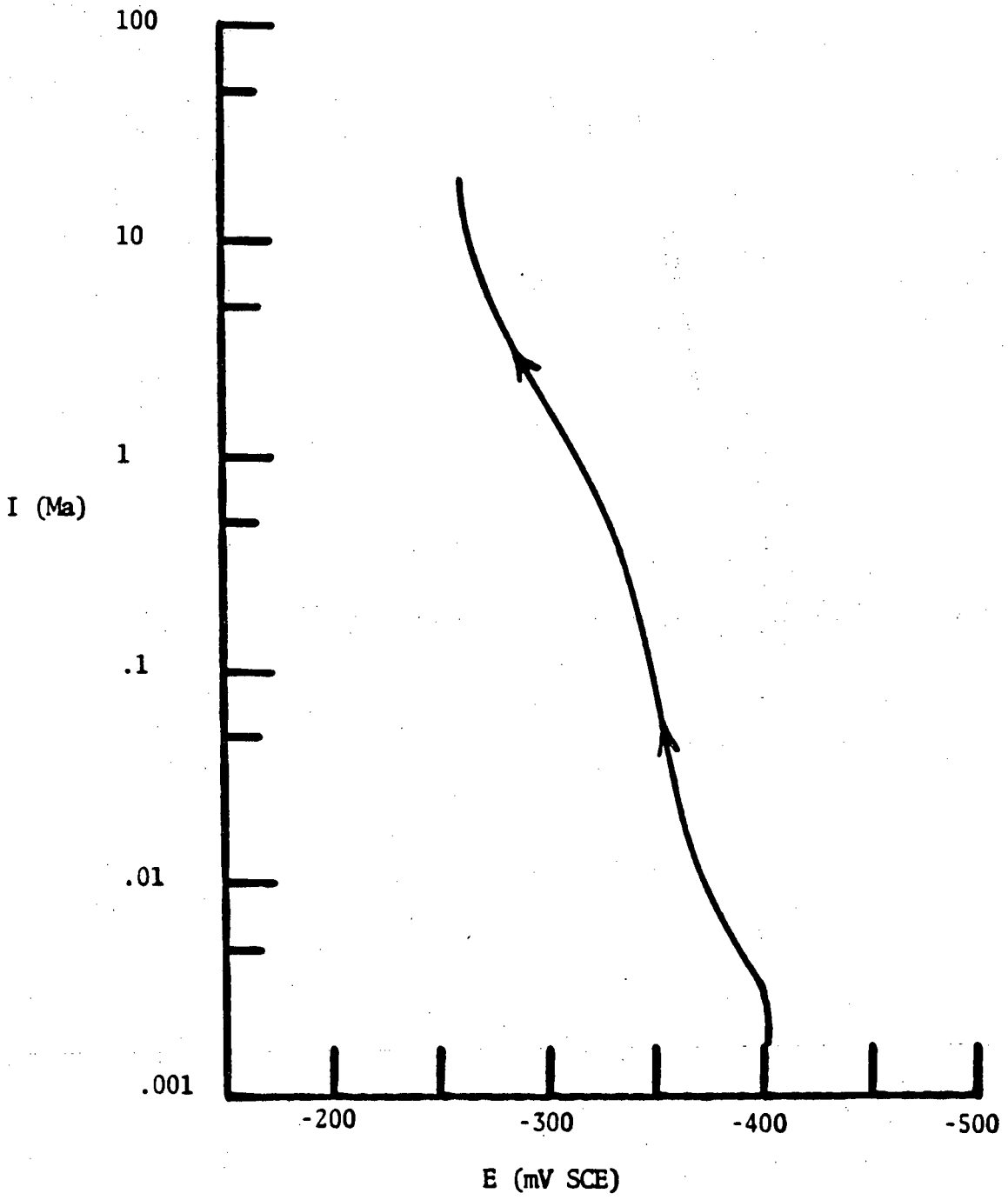

Fig. 10: Polarization Curve; 4.9M NaCl, pH = 6.0, 107°C.

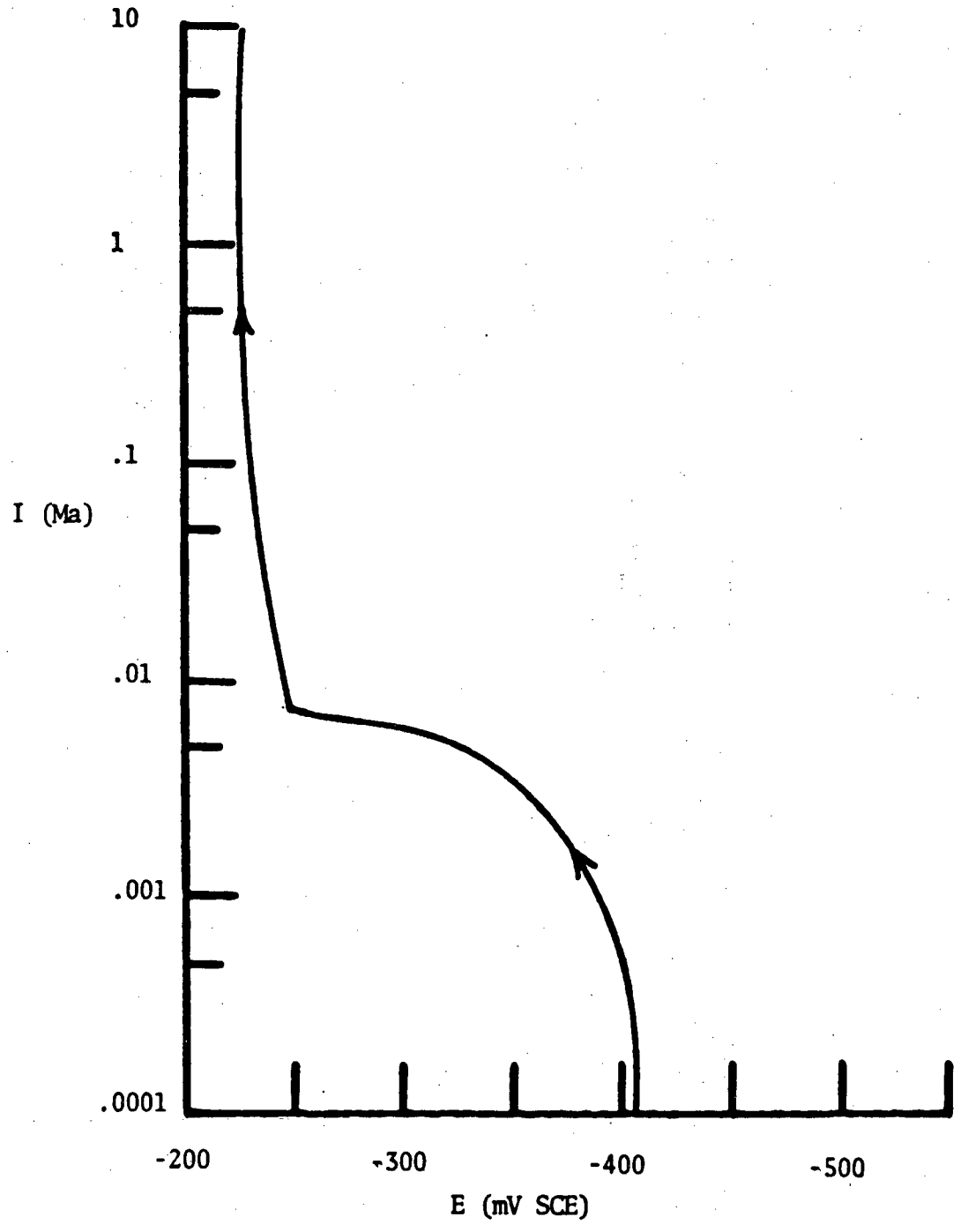

Fig. 11: Polarization Curve; 4.9M NaCl, .15M Na_2SO_4, pH = 6.0, 107°C.

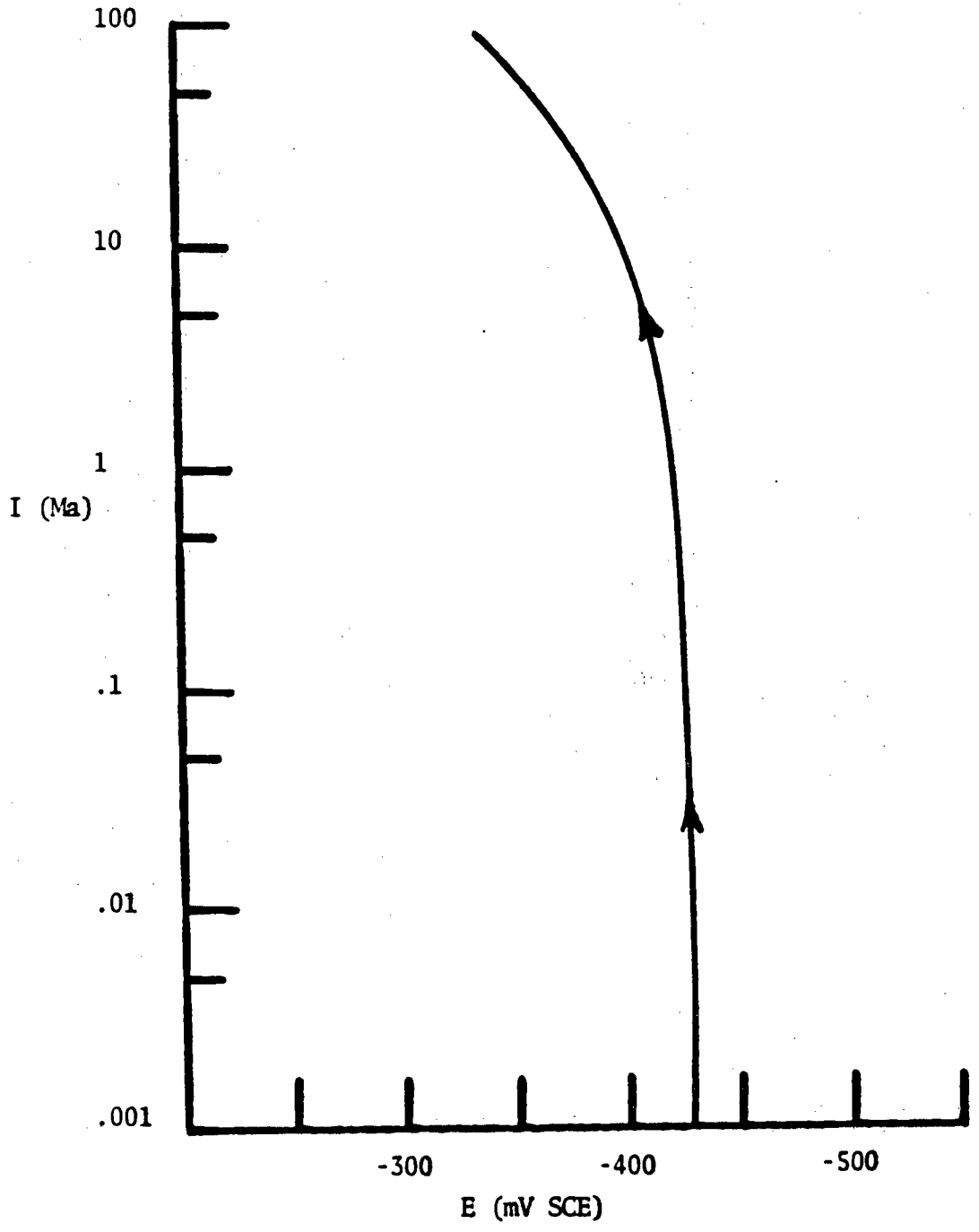

Fig. 12: Polarization Curve; 4.9M NaCl, 2.0 ml HCl/lt, pH = .7, 107°C.

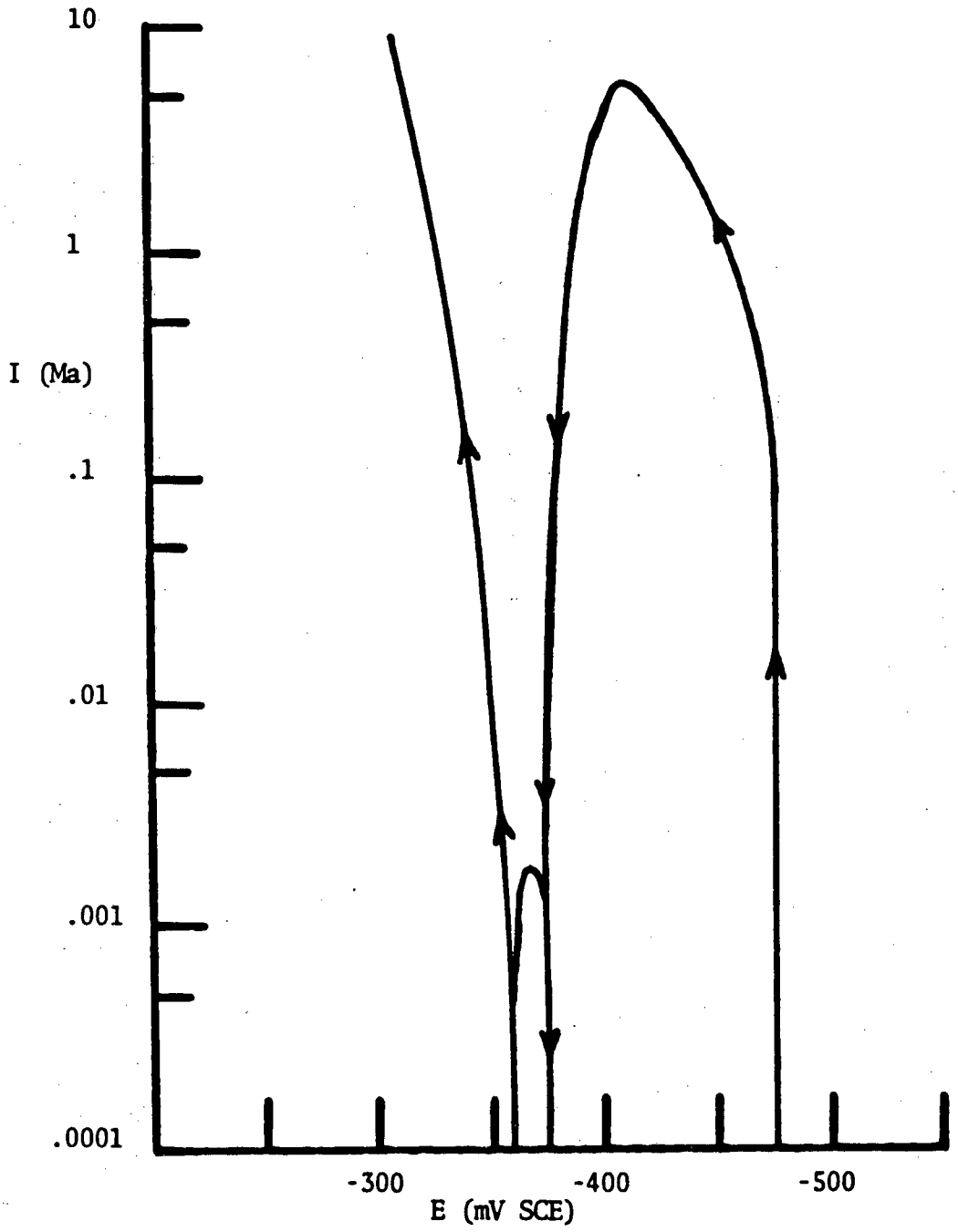

Fig. 13: Polarization Curve; 4.9M NaCl, .15M NaCl, 1.0 ml HCl/1t, pH = 1.25, 107°C.

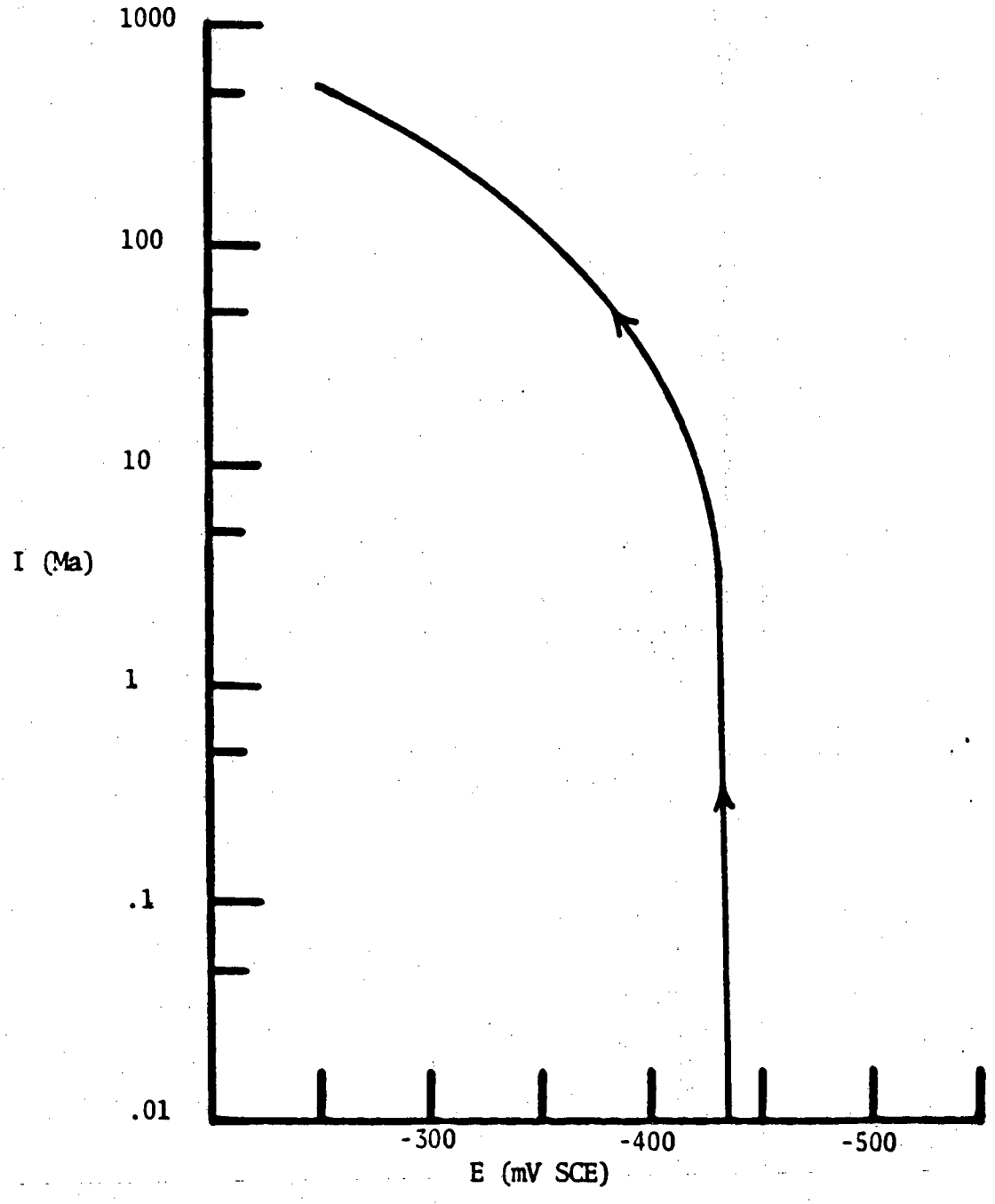

Fig. 14: Polarization Curve; 4.9M NaCl, .15M Na_2SO_4, 3.0 ml HCl/1t, pH = .35, 107°C.

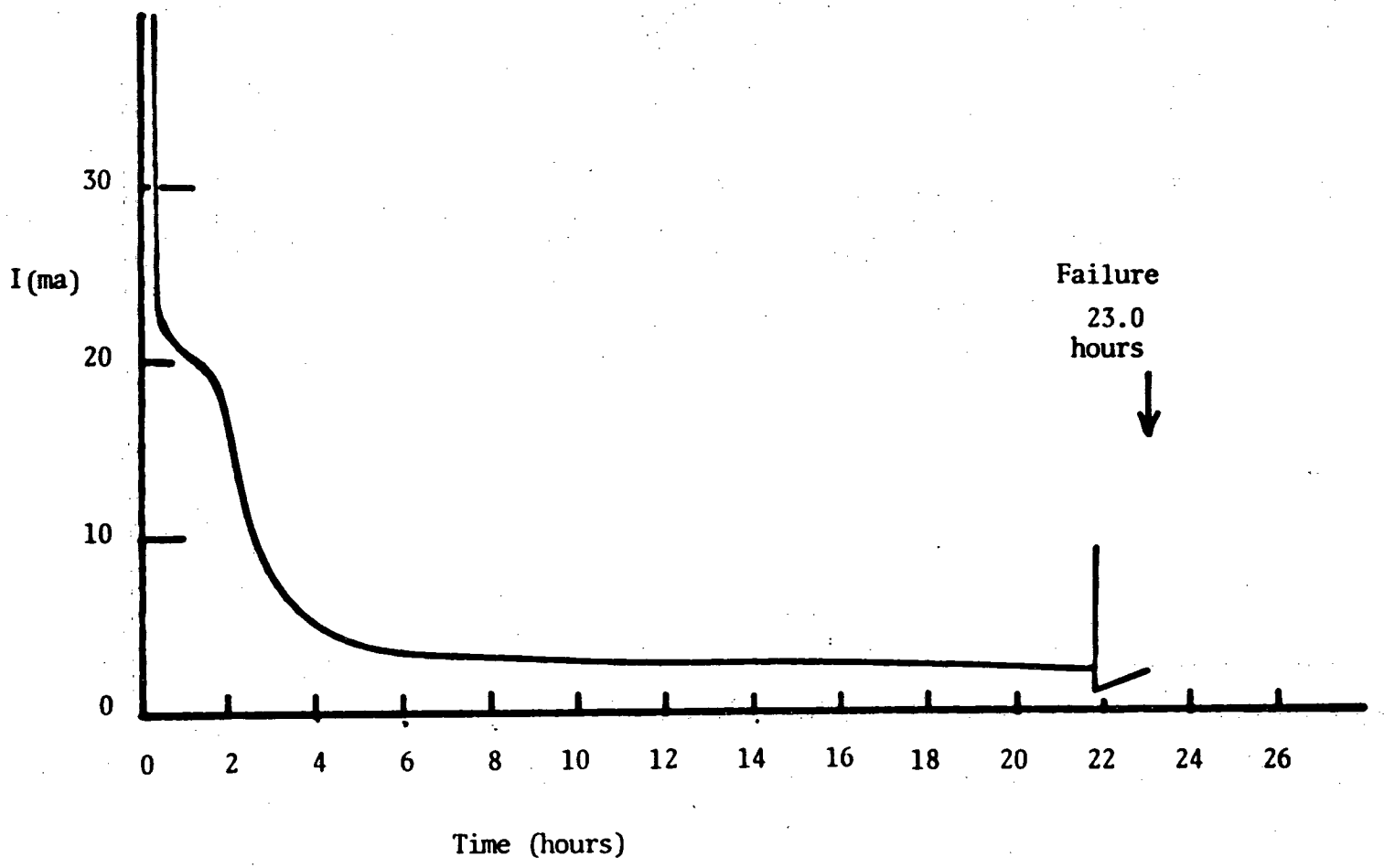

Fig. 15: Current vs. Time, Annealed, Applied Potential = -370 mV, 4.9 M NaCl, .15 M Na_2SO_4, 3 ml HCl/1t, initial pH = .51, final pH = .65, 107°C.

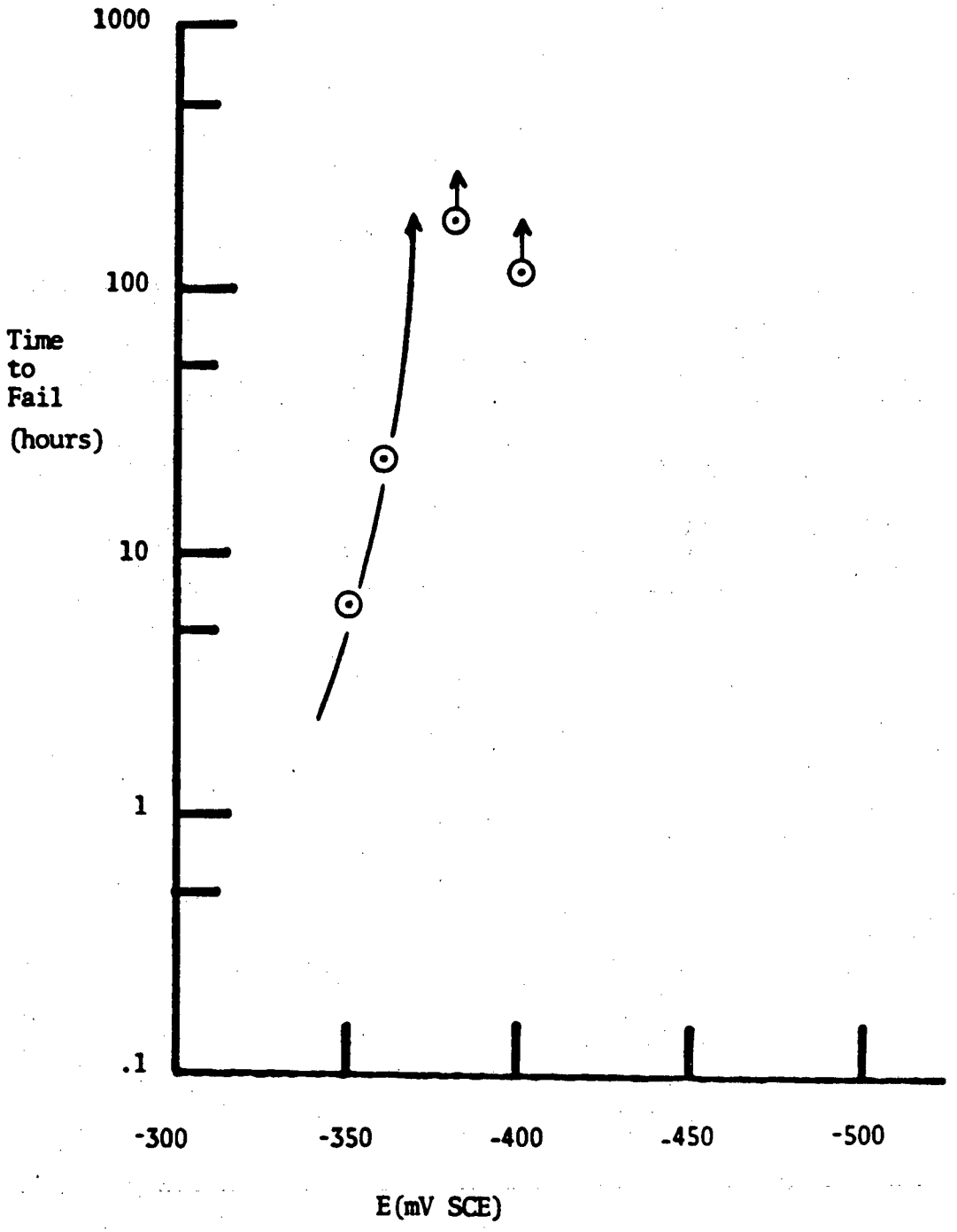

Fig. 16: Time to Fail vs. Potential; Annealed, 4.9 M NaCl, .15 M Na_2SO_4, 3 ml HCl/1t, 107°C.

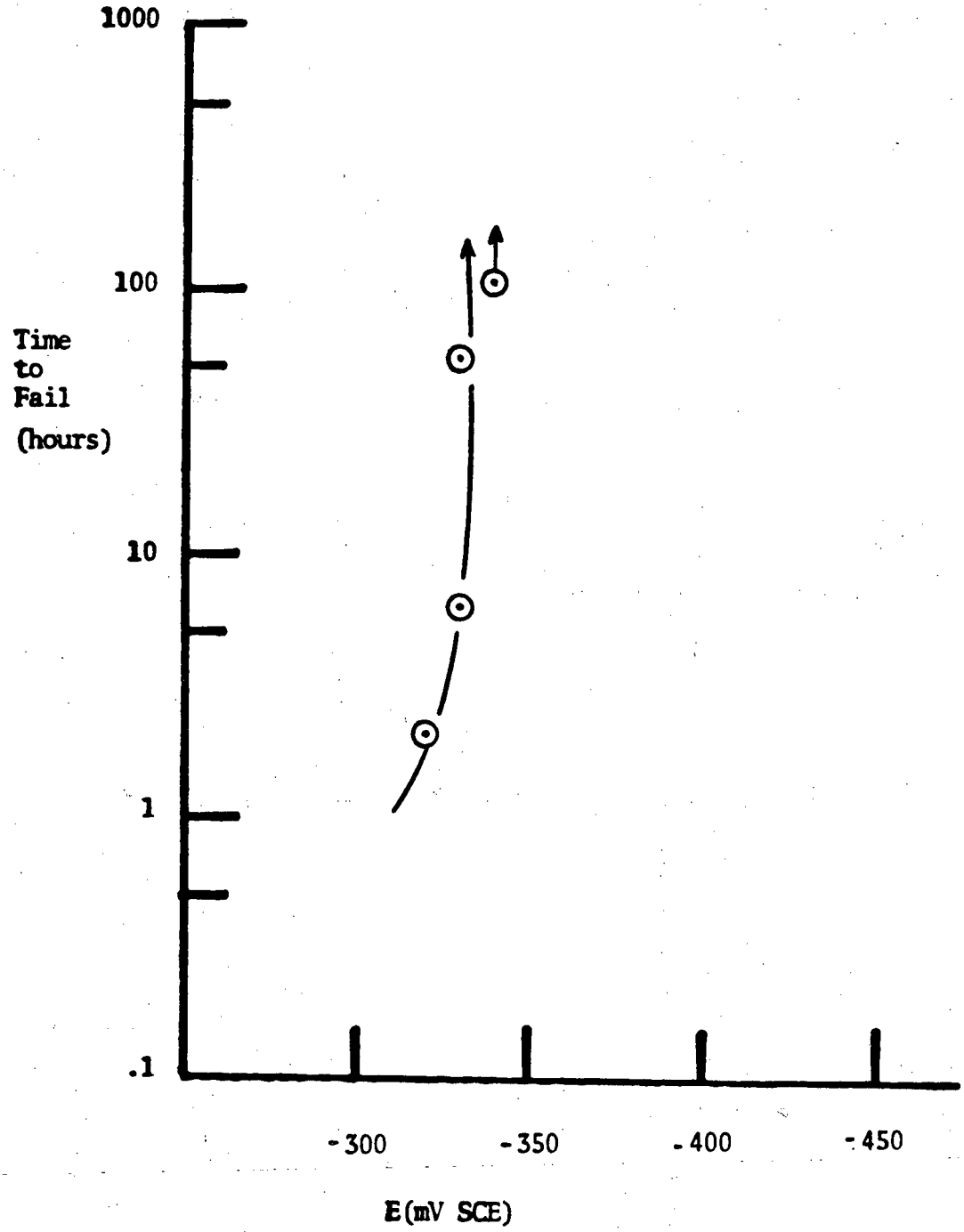

Fig. 17: Time to Fail vs. Potential, 25% Cold Rolled, 4.9 M NaCl, .15 M Na_2SO_4, 3 ml HCl/1t, 107°C.

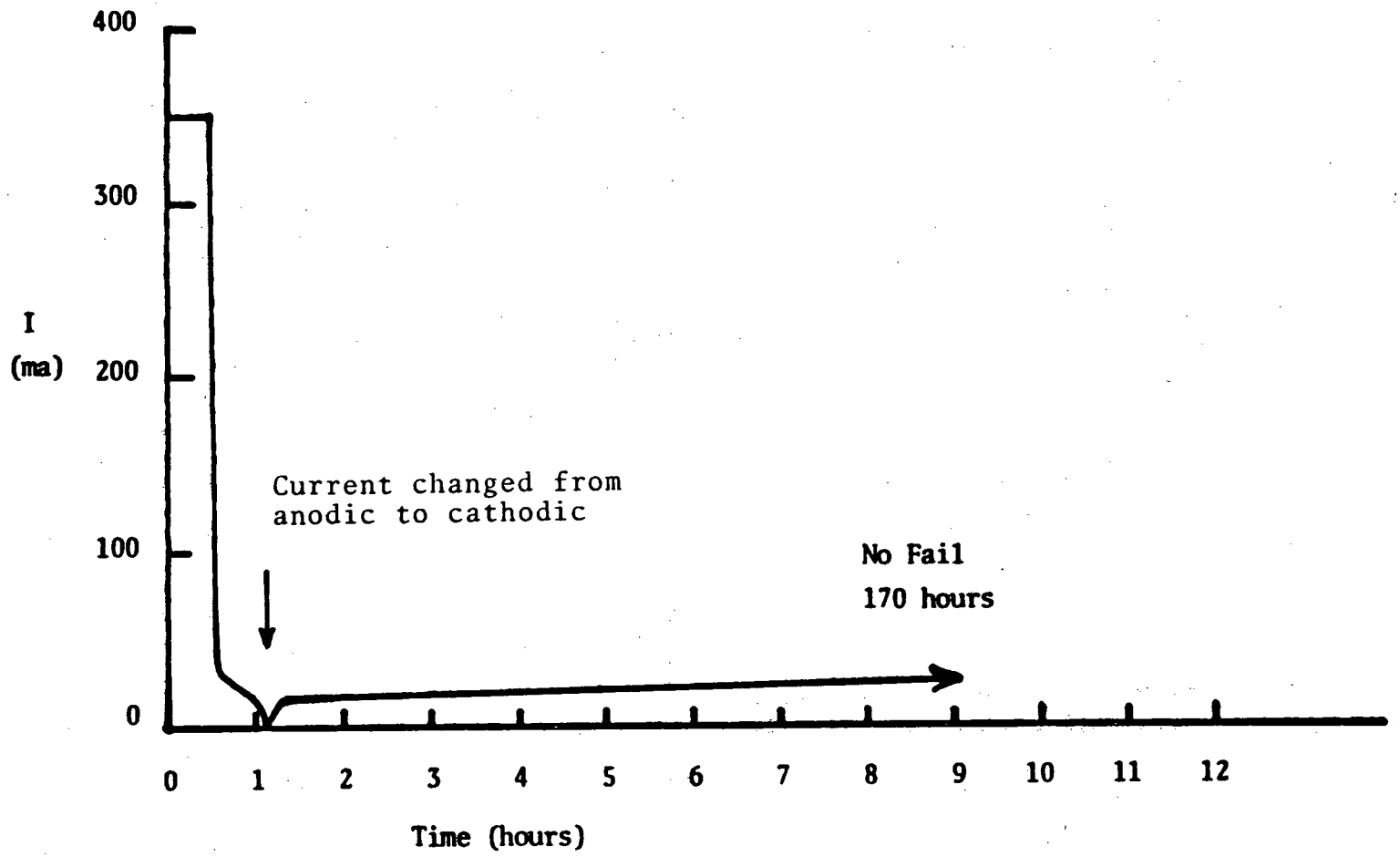

Fig. 18: Current vs. Time; Annealed, Applied Potential = -380 mV, 4.9 M NaCl, .15 M Na_2SO_4, 3.0 ml HCl/1t, initial pH = .60, final pH = 1.20, 107°C.

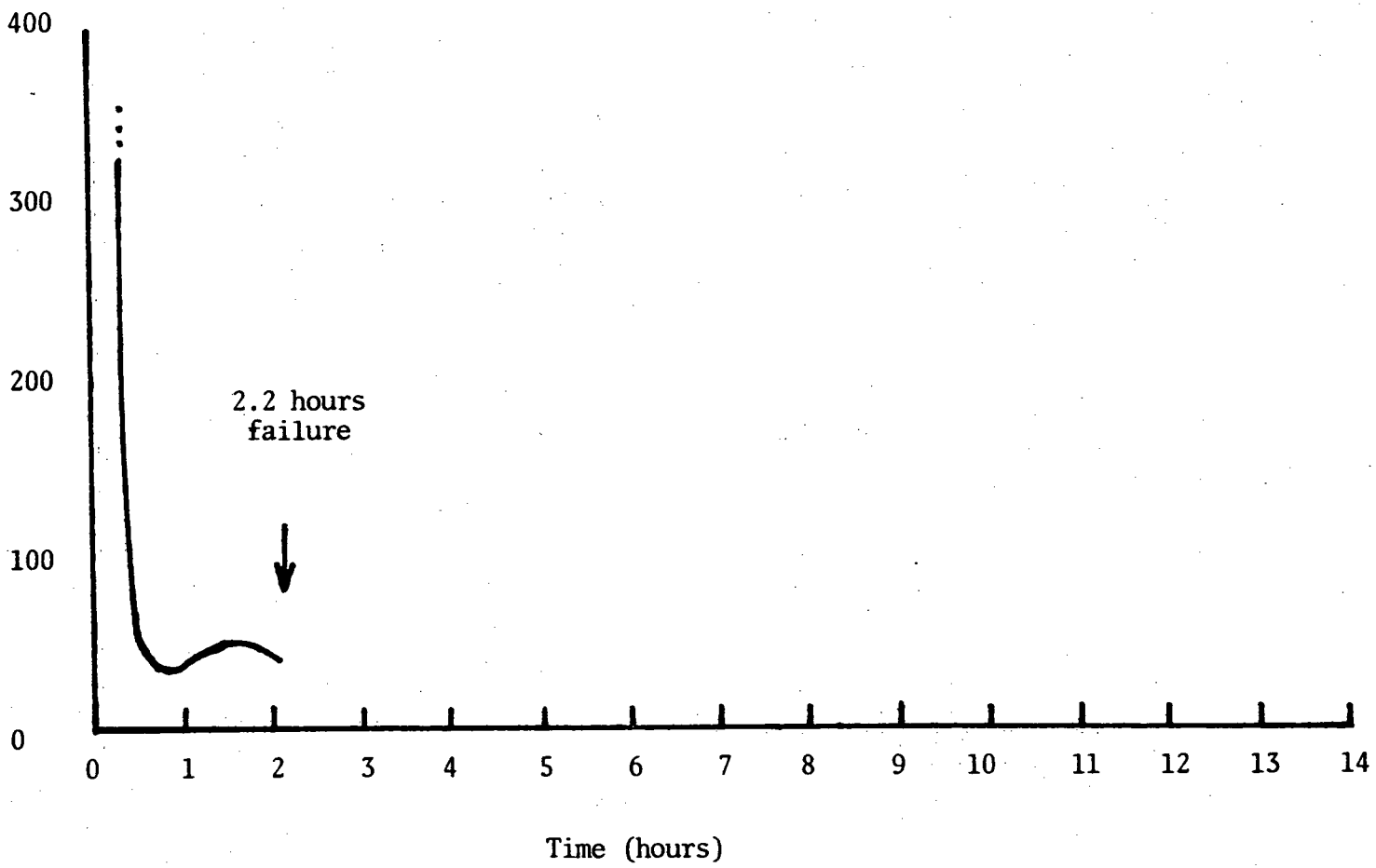

Fig. 19: Current vs. Time; 25% Cold Rolled, Applied Potential = -370 mV, 4.9 M NaCl, .15 M Na_2SO_4, 3.0 ml HCl/1t, initial pH = .71, final pH = 1.45, 107°C.

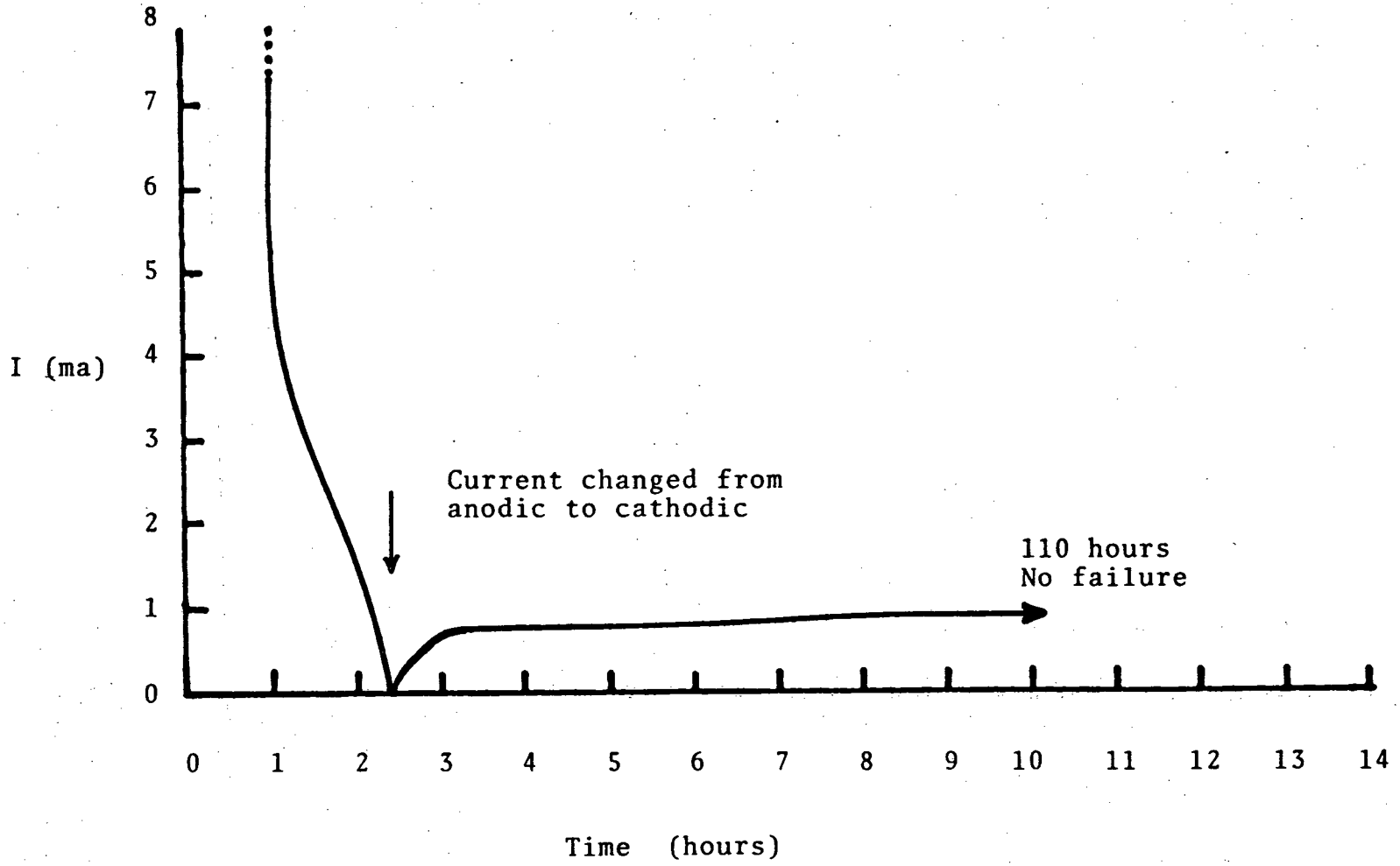

Fig. 20: Current vs. Time; 25% Cold Rolled. Applied Potential = -390 mV, 4.9 M NaCl, .15 M Na_2SO_4, 3.0 ml HCl/1t, initial pH = .60, 107°C.

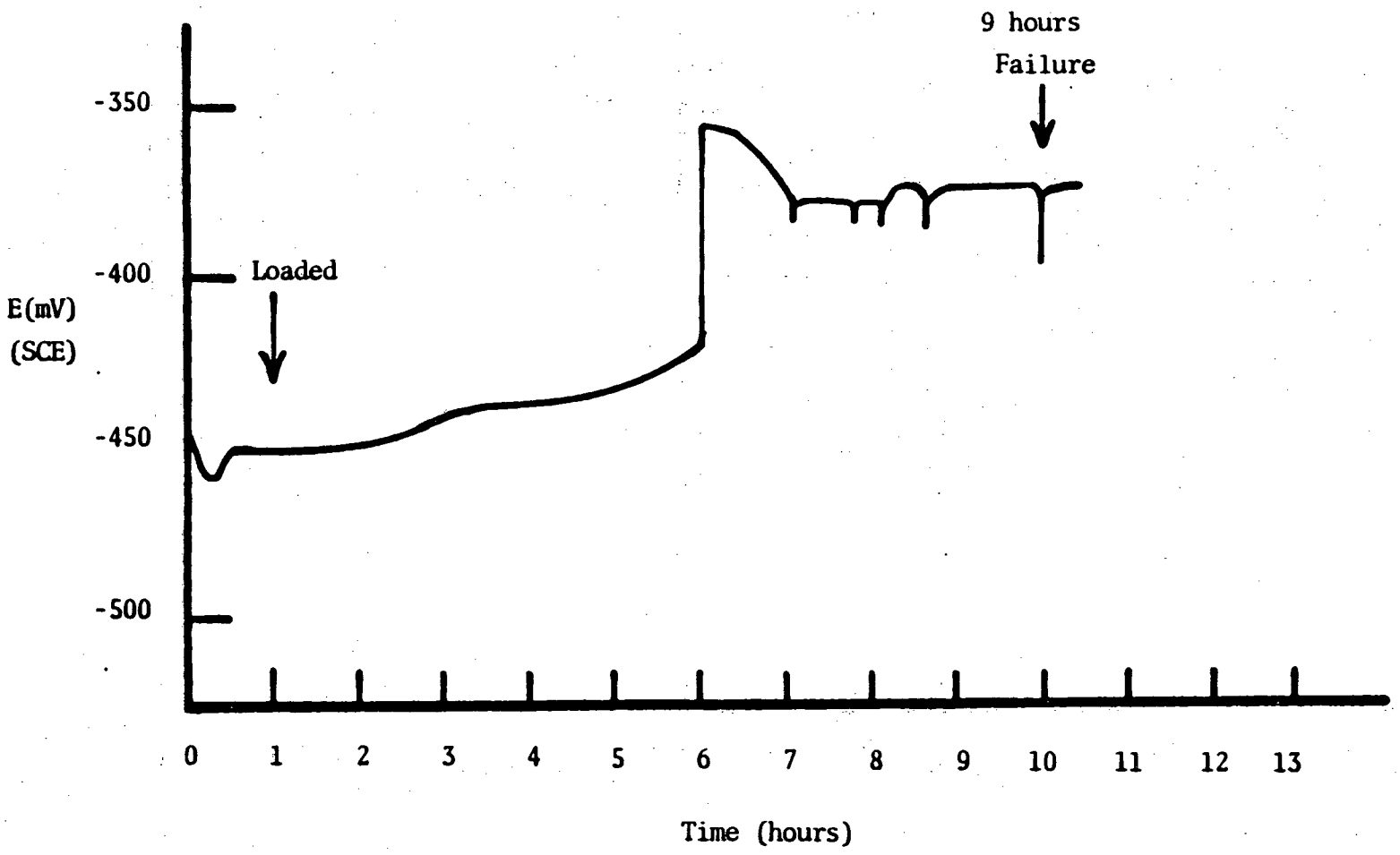

Fig. 21: E_{oc} vs. Time; 25% Cold Rolled, 4.9 M NaCl, .15 M Na_2SO_4, 3.0 ml HCl/1t, initial pH = .5, final pH = 1.3, 107°C.

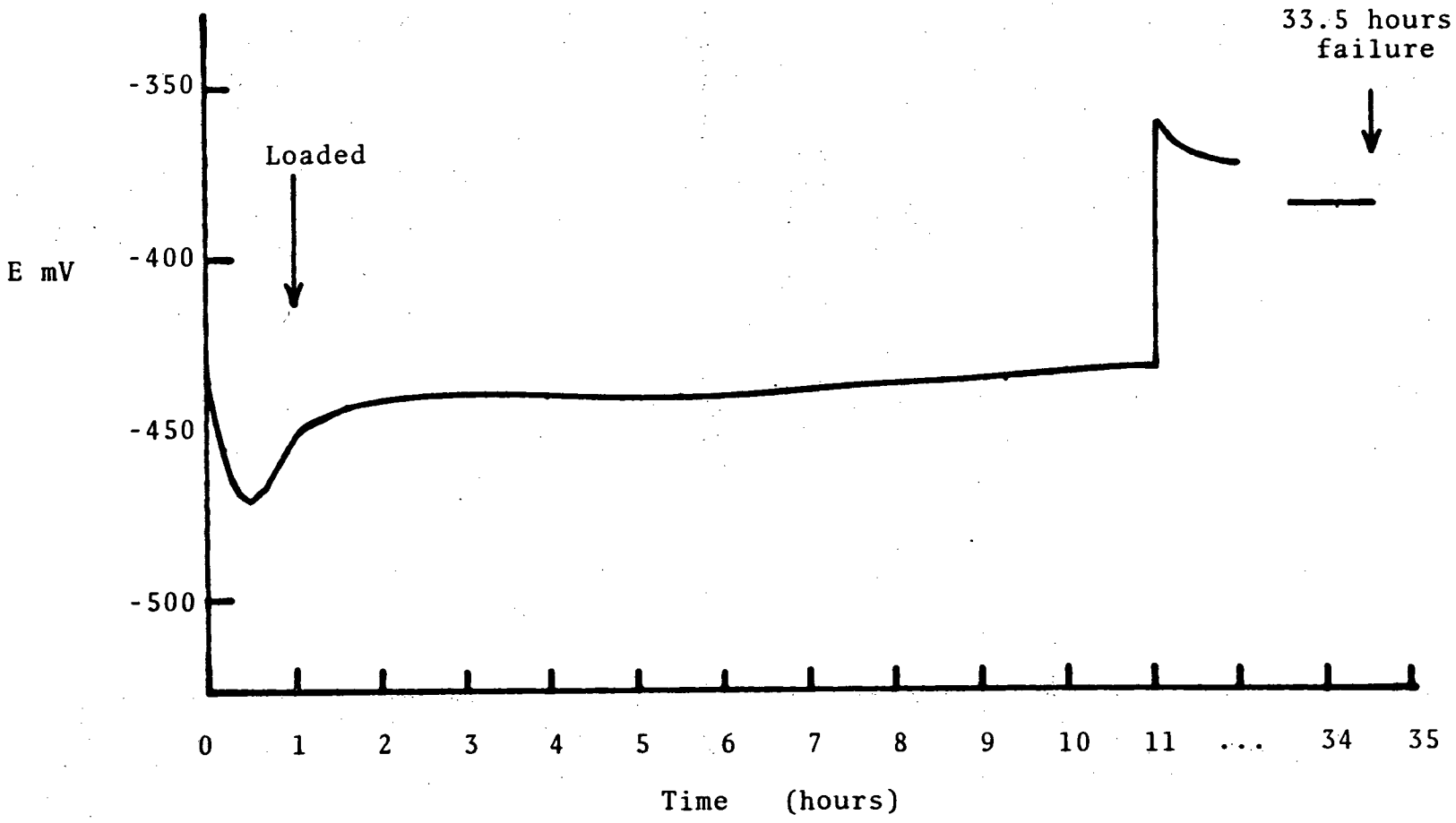

Fig. 22: E_{oc} vs. Time, Annealed; 4.9 M NaCl, .15 M Na_2SO_4, 3.0 ml HCl/1t, initial pH = .75, final pH = 1.45, 107°C.

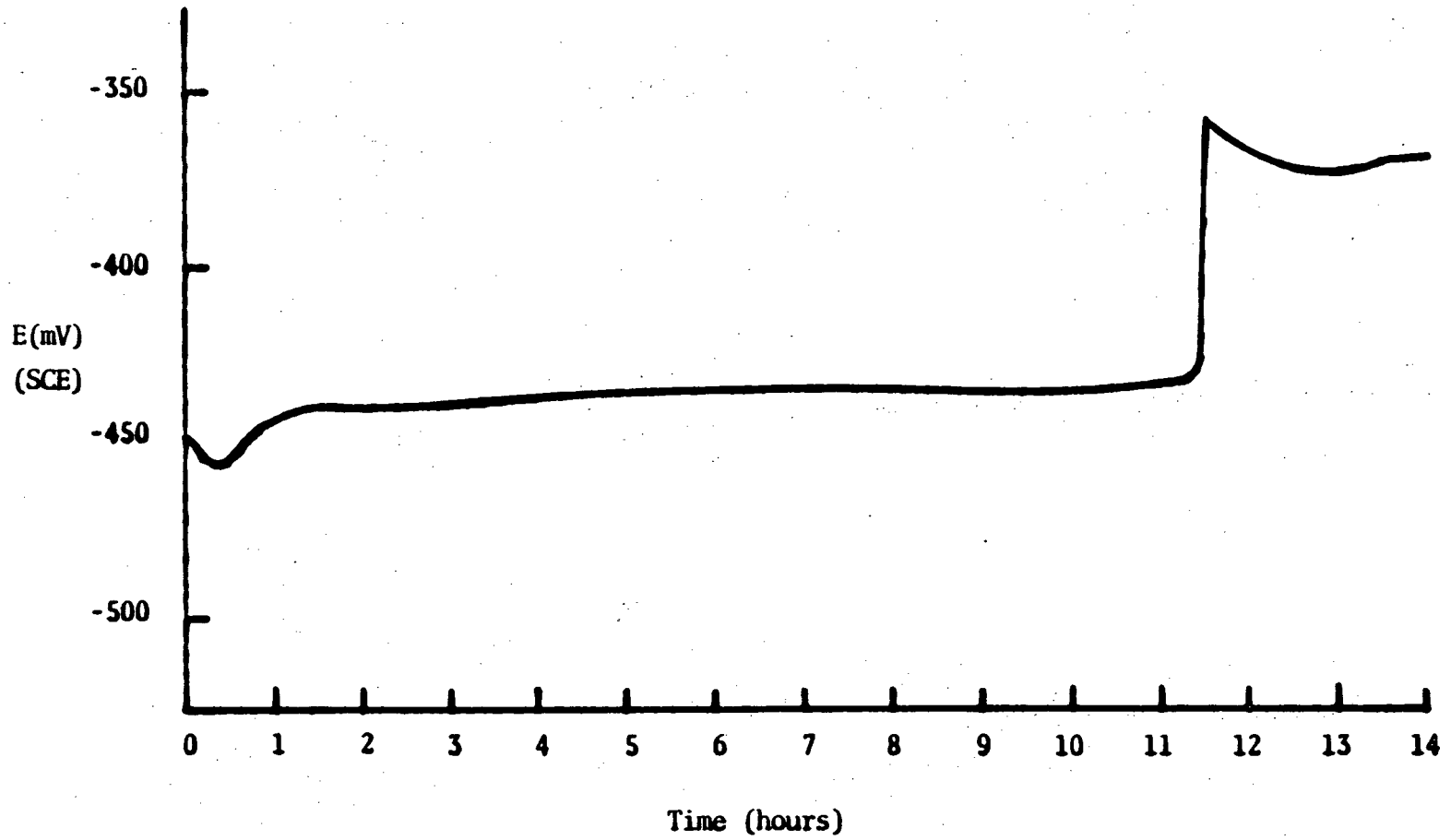

Fig. 23: E_{oc} vs. Time. Without applied Stress; 4.9 M NaCl, .05 M Na_2SO_4, 3.0 ml HCl/1t, initial pH = .6, final pH = 1.4, 107°C.

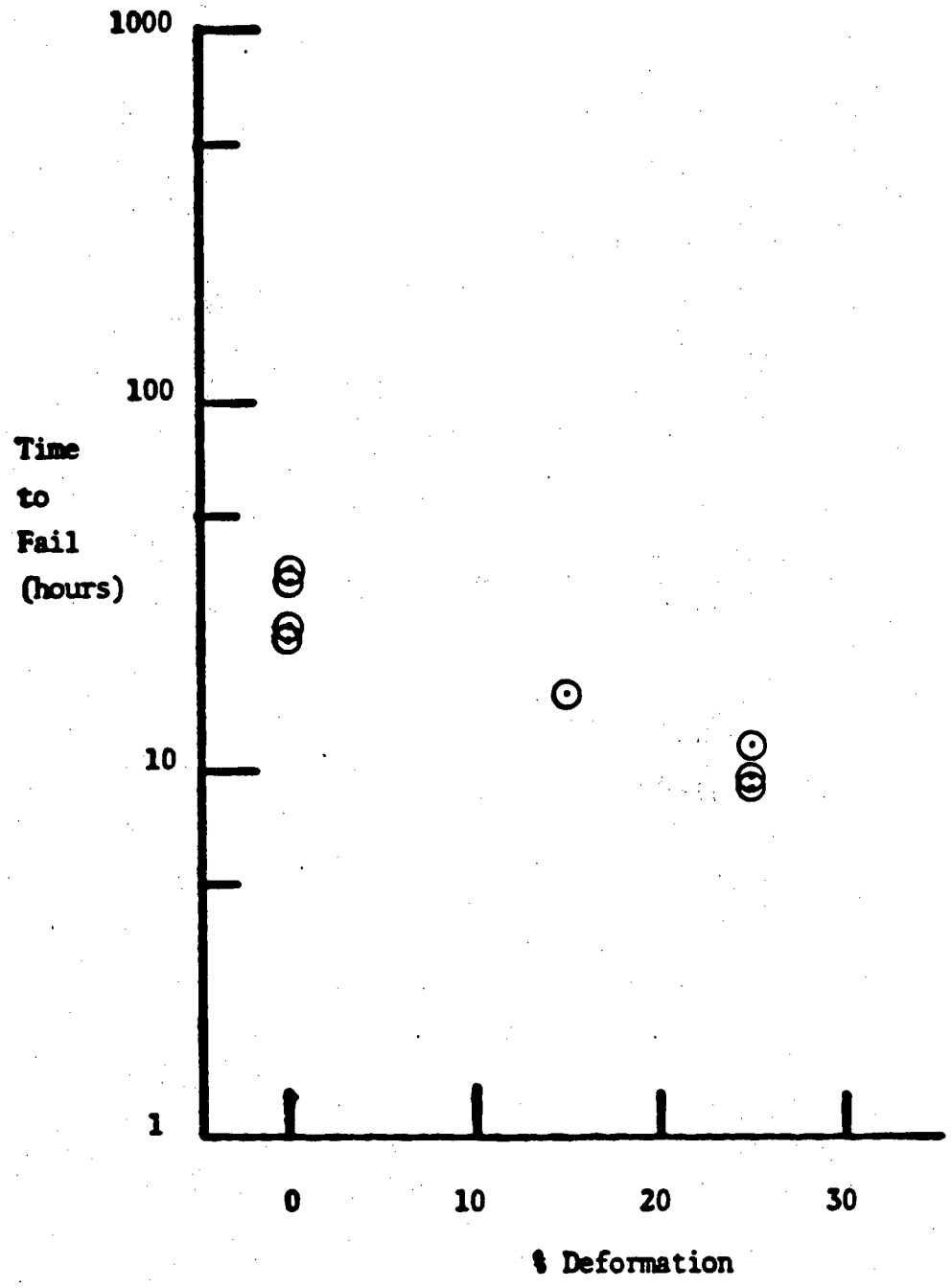

Fig. 24: Time to Fail vs. % Deformation. Open Circuit, 4.9 M NaCl, .15 M Na_2SO_4, 3.0 ml HCl/1t, 107°C.